Impact of in-pore salt crystallization on transport properties

Author(s):
Espinosa-Marzal, R. M.; Scherer, G. W.

ORIGINAL ARTICLE

Impact of in-pore salt crystallization on transport properties

Rosa M. Espinosa-Marzal · George W. Scherer

Abstract Precipitation of salts in confined spaces is the key mechanism for rock weathering and damage to building materials. To date there is no comprehensive study of the parameters influencing the reduction of pore space by salt crystals and the consequences for transport and damage by crystallization pressure. A novel method is presented to quantify pore clogging (i.e., the degree to which crystallization of salts interferes with transport of solution in porous materials). After drying capillary-saturated stone specimens containing salt solutions, the rate of capillary uptake of decane into the salt-contaminated specimens is measured. By treating the salt-contaminated material as a bilayer, the width of the crystallization front and the degree of pore filling can be determined. Two model materials with different pore size distributions (Indiana and Highmoor limestone) and three salts (sodium chloride, sodium sulfate and magnesium sulfate) are selected for this study. It is shown that pore clogging results from the interplay between pore size distribution and salt properties. Different scenarios are discussed to link pore clogging with salt damage.

R. M. Espinosa-Marzal (✉)
Laboratory for Surface Science and Technology,
Department of Materials, ETH Zurich,
Wolfgang-Pauli-Strasse 10, 8093 Zurich, Switzerland
e-mail: rosa.espinosa@mat.ethz.ch

R. M. Espinosa-Marzal · G. W. Scherer
Civil and Environmental Engineering/PRISM,
Princeton University, Eng. Quad. E-319, Princeton,
NJ 08544, USA
e-mail: scherer@princeton.edu

Introduction

Precipitation of crystals in a porous network reduces the permeability of the system, resulting in negative effects in situations as diverse as deterioration of monuments (Goudie and Viles 1997; Steiger and Siegesmund 2007), extraction of hydrocarbons from geological formations (Kirk and Dobbs 2002), and functioning of kidneys (Wesson et al. 1998).

Salts, such as de-icing salts, may be carried into stone with ground water by capillary rise, leach from mortar joints, or result from the chemical reaction between atmospheric pollution (especially SO_2) and minerals (such as calcite, $CaCO_3$, in limestone). Evaporation of water or a drop in temperature may result in supersaturation of the pore solution, leading to in-pore precipitation of salt. If evaporation occurs in a film of solution on the surface of the stone, then the crystals form a harmless (but unattractive) external deposit called "efflorescence". However, if salts precipitate beneath the material surface (a phenomenon called subflorescence or crypto-florescence), severe damage can result, if the crystallization pressure (Correns 1949; Flatt et al. 2007; Steiger 2005a, b) exceeds the tensile strength of the material. Thus, salt crystallization is directly involved in degradation of construction materials, such as concrete, brick and natural stone, and is responsible for severe damage of historic architecture, civil structures, roads, highways, runways, dams and tunnels.

Salt weathering in the field can only be understood if the interaction between stone properties, environmental conditions and composition of the salt mixtures and fluid phases are considered; even in a simple laboratory experiment, this requires numerical modeling. Numerical and analytical models have been developed to describe ion transport in porous materials (e.g., Samson and Marchand

2007; Sghaier et al. 2007; Guglielmini et al. 2008; Huinink et al. 2002), including coupling to poromechanical models (Espinosa-Marzal and Scherer 2009) to estimate the stress from crystallization. However, we still have inadequate knowledge of the kinetics of crystallization of crystals within the pore network, the influence of efflorescence and subflorescence on the transport of the solution, film effects (Prat 2007), and the properties of the confined film of solution between the salt and mineral surfaces (Scherer 2004). Nuclear magnetic resonance measurements of water content and dissolved salt during the one-sided drying of brick samples saturated with sodium chloride (SC, NaCl) illustrate the competition between advection to the surface and redistribution by diffusion (Pel et al. 2002), and preferential crystallization at the surface for high Peclet-number values. Shokri et al. (2010) obtain similar trends for sand columns by pore-scale X-ray synchrotron measurements, and show that large pores are invaded rapidly by air, whereas fine pores remain saturated and act as evaporating sites. Studies in model porous materials made by glass beads show that efflorescence of NaCl first accelerates evaporation due to a capillary pumping effect, then decreases the drying rate as the efflorescence dries out and acts as an additional barrier for the diffusive transport (Sghaier and Prat 2009). In the absence of efflorescence, the measured decrease of the drying rate of limestone saturated with NaCl and magnesium sulfate (MS, $MgSO_4$) solutions, when compared to salt-free limestone, was related to solution viscosity and to volume fraction occupied by the salt crystals (Espinosa-Marzal and Scherer 2008a).

In-pore crystallization causes a reduction of the volume, which hinders solution transport, a phenomenon that we call pore clogging. Since pore clogging affects the location and quantity of crystals, it might have implications for the stress development and deterioration of the material. The need to elucidate this phenomenon inspired the present work.

Sodium sulfate (SS, Na_2SO_4) has an exceptional ability to cause damage to porous materials and several works have investigated the mechanism of damage (Goudie and Viles 1997; Scherer 2004; Rodriguez-Navarro and Doehne 1999; Ruiz-Agudo et al. 2007; Espinosa-Marzal et al. 2011; Espinosa-Marzal and Scherer 2008a; Shahidzadeh-Bonn et al. 2010; Flatt 2002), while NaCl is often related to damage of monuments in the Mediterranean Basin and to rock weathering in deserts (Goudie and Viles 1997). $MgSO_4$ is also commonly related to weathering processes on Earth (Evans 1969). Laboratory experiments confirm that MS is capable of causing the stone to fracture (Ruiz-Agudo et al. 2007). Recent research on the intense damage of dolomitic limestone was found to be related to phase changes of MSs salts in the pores of the stone (Lopez-Arce

et al. 2009; Doehne and Pinchin 2008); three stable phases and at least eight metastable phases have been found on Earth, which suggests the complexity of damage mechanisms by this salt. A possible damage mechanism is the hydration of kieserite into hexahydrate in confined spaces as shown by Steiger et al. (2007) and fast drying (Balboni et al. 2011).

In this paper, we describe a method to estimate quantitatively the pore clogging by NaCl, Na_2SO_4 and $MgSO_4$ salts in two different limestones as a function of both pore structure and salt type. Width of the crystallization front and pore filling are calculated using a model developed by Hall and Hoff (2002) to infer permeability of bilayer composites from the kinetics of liquid sorption. This method has been recently used to describe the capillary water uptake in masonries under the influence of mortar joins and validated by X-ray visualization of the wet front (Janssen et al. 2012). We use decane for imbibition, because it does not dissolve or hydrate the salts. We will show that pore clogging is strongly dependent on the type of salt and the pore structure of the porous host.

Analysis of the sorptivity of a bilayer composite

The purpose of this analysis is to quantify the width of the crystallization front and the pore filling within the front by measuring the liquid uptake into a salt-contaminated material. Following Hall and Hoff (2002), we write the equations in terms of the quantity $K = k/\eta$, where k is the intrinsic permeability (units of area) and η is the viscosity (units of Pa s); for convenience, K will be called the permeability. Consider a composite consisting of two materials A and B with different permeabilities (K_A and K_B, respectively), different sorptivities (S_A and S_B), and different effective porosities (f_A and f_B). The effective porosity gives the pore volume filled with the absorbed liquid in the wet region. Layer A is in contact with liquid at the free surface ($z = 0$) and the boundary between A and B is at $z = L_A$, as shown schematically in Fig. 1.
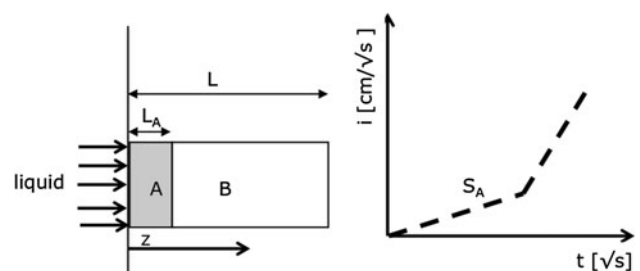

Fig. 1 Schematic representation of the bilayer composite and the imbibition

Hall and Hoff ([2002](#)) give the imbibition rate, i, for the composite as:

$$i = S_A t^{1/2}, \quad z < L_A$$
$$i = S_B \left(t + L_A^2 \left(\left(\frac{f_B}{S_B} \right)^2 \left(\frac{K_B}{K_A} \right)^2 - \left(\frac{f_A}{S_A} \right)^2 \right) \right)^{1/2} \tag{1}$$
$$- L_A \left(f_B \frac{K_B}{K_A} - f_A \right), \quad z > L_A,$$

where the relation between the imbibition i and the advancing wet front, z, is given by

$$i = z f_A, \quad z < L_A$$
$$i = L_A f_A + f_B (z - L_A), \quad z > L_A. \tag{2}$$

Applying Darcy's law to describe the capillary uptake and assuming a sharp front between the wet and the dry region, it can be shown that the sorptivity (m³ liquid/m² surface s$^{-1/2}$) is given by

$$S = \sqrt{2 f_e K \Psi_c}, \tag{3}$$

where K is the permeability in (m³s/kg), f_e the effective porosity and ψ_c the driving force for the capillary uptake, which is given by the Laplace equation:

$$\psi_c = \frac{2\gamma}{r}, \tag{4}$$

where γ is the liquid–vapor interfacial energy and r is the capillary radius, assumed to be an average pore radius of the stone.

For our application, A is the porous stone with salt in the pores and B the salt-free stone. The position of the boundary between A and B (i.e., the depth of the crystallization front) is unknown, as is the pore filling with crystals, the permeability and the sorptivity of A; however, an estimate of the pore filling is obtained by assuming that the salt is distributed uniformly only in material A. Thus, if the volume fraction of salt in A is ϕ_c^A (in m³/m³), then the effective porosity of A is given by

$$f_A = f_B - \phi_c^A \tag{5}$$

which corresponds to a pore filling (or, crystal saturation), s_c, with respect to the salt-free material of

$$s_c = \phi_c^A / f_B. \tag{6}$$

The simplest way to describe the reduction of pore radius due to the precipitated crystals corresponding to $f_A = f_B - s_c f_B$ is to attribute a characteristic pore size to each region and assume that those sizes differ according to the volume fraction of salt:

$$r_A = r_B (1 - s_c)^n \tag{7}$$

with $n = 1/3$ for spherical and $n = 1/2$ for cylindrical pores. This is a rough approximation, because the salt might be preferentially located in the smallest pores, or deposited as a layer of uniform thickness in pores of all sizes, and each distribution would result in a different effective size. Having no detailed information about the distribution of salt, we adopt the simplest approach, as expressed in Eq. ([7](#)).

According to the Carman–Kozeny equation (Happel and Brenner [1983](#)), the permeability can be approximated by

$$K \approx \frac{f_e r^2}{20\eta}. \tag{8}$$

This equation provides a good estimation of the permeability of the selected saturated stones with r equal to the average pore radius measured by mercury porosimetry. Thus, the relation between K_A and K_B follows from:

$$K_A = K_B (1 - s_c)^m \tag{9}$$

with $m = 2n + 1$, which is 5/3 for spherical and 2 for cylindrical pores. Similarly, the change of the driving force is given by

$$\Psi_A = \Psi_B / (1 - s_c)^n. \tag{10}$$

According to Eqs. ([5](#)), ([6](#)), ([9](#)) and ([10](#)), the relation between the sorptivity of A and B is

$$S_A = S_B (1 - s_c)^{\frac{m+1-n}{2}}. \tag{11}$$

Assuming a uniform salt distribution within the crystallization front, the total volume fraction occupied by salt in A is

$$\phi_c^A = \frac{\phi_c L}{L_A}, \tag{12}$$

where $L = L_A + L_B$ is the thickness of the stone and ϕ_c is the average volume fraction of salt in the material. Therefore, the saturation can be written as

$$s_c = \frac{\phi_c L}{f_B L_A}. \tag{13}$$

Substituting Eqs. ([5](#)), ([6](#)) and ([11](#))–([13](#)) into Eq. ([1](#)),

$$i = S_B (1 - s_c)^{n+2} t^{1/2}, \quad z < L_A$$
$$i = \left(S_B^2 t + (L_A f_B)^2 \left((1 - s_c)^{-2(2n+1)} - (1 - s_c)^{-2(n+1)} \right) \right)^{1/2}$$
$$- L_A f_B \left((1 - s_c)^{-(2n+1)} - (1 - s_c) \right), \quad z > L_A. \tag{14}$$

Since S_B and f_B can be measured for the salt-free stone, and the average volume fraction of salt ϕ_c is known, the only unknown to determine from fitting $i(t)$ is the width of the crystallization front L_A

Materials and methods

Materials: stones and salts

Two limestones, Indiana Limestone (IL) and Highmoor magnesian limestone (HL), and three salts, SS, SC and MS, were selected for this study. The pore size distributions of the stones were measured by mercury intrusion porosimetry (WIN9400 Series, Micromeritics Instruments Corp., Atlanta, USA) on small pieces with a total mass of ∼2 g. The total porosity was determined by water impregnation under vacuum. For this purpose, five dry samples (10 × 5 × 5 mm) of IL and HL, respectively, with known initial mass, were evacuated in a desiccator for 8 h and then water was admitted into the desiccator until the samples were submerged. After 24-h immersion, the weight increase from water uptake in the stone samples was determined gravimetrically and converted into volume fraction. The same samples were then dried at 80 °C in an oven and afterwards placed back in a desiccator. The water uptake was determined in the same way without initial evacuation of the desiccator to determine the total porosity under atmospheric pressure.

The volume of the crystals was computed with the densities of the salt crystals given in Table 1 for halite (NaCl), hexahydrite ($MgSO_4 \cdot 6H_2O$), epsomite ($MgSO_4 \cdot 7H_2O$), kieserite ($MgSO_4 \cdot 1H_2O$), thenardite (Na_2SO_4) and mirabilite ($Na_2SO_4 \cdot 10H_2O$) (Lide 2006). The densities of the solutions saturated with respect to the different salts were calculated according to the Pitzer model (Steiger et al. 2008) and are given in the same table.

The thermodynamically stable SS salt at 21 °C and 31 % RH is the anhydrate, thenardite. Thenardite precipitates directly only if the concentration exceeds 3.63 m (molal, mole per kg water), which is promoted by a high evaporation rate. At low evaporation rates, both SS decahydrate (mirabilite) and SS heptahydrate ($Na_2SO_4 \cdot 7H_2O$) are observed to precipitate from the solution and dehydrate slowly to thenardite (Rodriguez-Navarro and Doehne 1999).

Kieserite is the stable phase of MS at 21 °C and 31 % RH, but crystallization of kieserite at these conditions has never been reported in the literature. Moreover, the dehydration of higher MS hydrates to kieserite is kinetically hindered at room temperature (Wang et al. 2009). Instead,

epsomite often precipitates at room temperature and dehydrates to hexahydrite and starkeyite ($MgSO_4 \cdot 4H_2O$). Indeed, although hexahydrite is thermodynamically stable only in the narrow temperature range from 47 to 71 °C, abundant efflorescence of hexahydrite is found in the field (Foster and Hoover 1963) and in laboratory experiments at room temperature (Steiger et al. 2007; Balboni et al. 2011).

Since the RH of the drying experiments is below the deliquescence humidity of halite, thenardite, mirabilite, epsomite, hexahydrite and kieserite, the hygroscopic behavior of the salt will not have any influence on the drying behavior.

Experimental methods

Stone prisms (5 × 2.5 × 2.5 cm) were soaked at room temperature for 15 h in water and in the following unsaturated salt solutions: 3.2 m NaCl (SC1) and 5.8 m NaCl (SC2), 0.85 m Na_2SO_4 (SS12), and 1.68 m $MgSO_4$ (MS20). After saturation with the solutions, five surfaces of the prismatic samples were coated with epoxy to prevent evaporation. The drying of the samples took place through one side (2.5 × 2.5 cm) at constant temperature 21 ± 1 °C and relative humidity 31 ± 2 %, while the weight loss was recorded. After reaching constant weight, efflorescences were removed and the uptake of decane through the uncoated surface was measured. Decane was used to avoid the dissolution of the precipitated salts in the pore liquid.

To investigate the crystallization behavior of the salts, drying of droplets (∼25 μl) of the solutions on a hydrophilic glass substrate was observed with a Nikon SMZ-U zoom microscope, using a cooling stage (Physitemp TS-4) to maintain a constant temperature, similar to previous experiments performed by Shahidzadeh-Bonn et al. (2008). A VGA2USB frame grabber (Epiphan systems) was connected to a digital camera (Nikon DS-SM) to record images of the time-dependent drying-induced crystallization. The droplet was pipetted onto a pre-cleaned cover glass. Some calcite powder was dispersed in the drop to simulate the heterogeneous nucleation in the pores of limestone. Similar drying experiments were performed in Petri dishes containing a larger amount of solution (∼90 ml). Accompanying drying experiments were performed at the same temperature and RH and with the same initial amount of solution (25 μl and 90 ml, respectively) to determine

Table 1 Density (in g/cm^3) of the salt crystals (ρ_c) considered in this study and of the solutions saturated with respect to the different salts at 21 °C (ρ_{sol}), and solubility (c_{sat}, in mol/kg) of the different salt crystals at 21 °C

	NaCl	$MgSO_4 \cdot 6H_2O$	$MgSO_4 \cdot 7H_2O$	$MgSO_4 \cdot 1H_2O$	Na_2SO_4	$Na_2SO_4 \cdot 10H_2O$
ρ_c	2.16	1.72	1.68	2.66	2.68	1.46
ρ_{sol}	1.20	1.36	1.29	1.51	1.35	1.16
c_{sat}	6.14	3.67	2.85	6.15	3.63	1.46

gravimetrically the rate of mass loss (and change in concentration) with a resolution of 1 mg.

Calculation of the average salt and water content in stone

After impregnation with the salt solution, the total mass of solution in the stone specimen $m_{sol,0}$ was determined gravimetrically. It consists of the initial masses of water $m_{w,0}$ and dissolved salt $m_{s,0}$:

$$m_{sol,0} = m_{w,0} + m_{s,0}. \tag{15}$$

If c is the concentration of the solution in g per 100 g water, then

$$m_{w,0} = \frac{m_{sol,0}}{1 + c/100} \quad \text{and} \quad m_{s,0} = \frac{cm_{sol,0}}{100 + c}. \tag{16}$$

At the end of the drying experiment, the pores contained salt crystals and solution with known total mass m^* obtained gravimetrically. Efflorescences were removed and their mass determined gravimetrically (m_{eff}). The final mass of salt in the stone, m_s, was also known

$$m_s = m_{s,0} - m_{eff}, \tag{17}$$

so the mass of remaining water m_w^{exp} was found from

$$m_w^{exp} = m^* - m_s. \tag{18}$$

It can be expected that the solution was saturated at the end of the drying experiment, so the amount of dissolved salt is

$$m_{diss} = \frac{c_{sat} m_{w,sol}}{100}, \tag{19}$$

where $m_{w,sol}$ is the mass of liquid water, and c_{sat} is the solubility (in g per 100 g water). The hydration water bonded to the salt crystals $m_{w,c}$ is given by:

$$m_{w,c} = \frac{m_{c,H} n_w M_w}{M_{anh}}, \tag{20}$$

where n_w is the number of water molecules in a formula unit of salt, M_w the molar mass of water, M_{anh} the molar mass of the anhydrous salt, and m_c is the mass of the salt forming part of the crystals (hydrated $m_{c,H}$ and anhydrous $m_{c,A}$). Thus,

$$m_c = m_s - m_{diss} = m_{c,H} + m_{c,A}. \tag{21}$$

The mass of residual water m_w^{exp} is given by the sum of $m_{w,c}$ and $m_{w,sol}$. Substituting Eqs. (16)–(20) into Eq. (21), it follows for the mass of hydrated precipitated salt

$$m_{c,H} = \frac{m_s - c_{sat}/(100 m_w^{exp}) - m_{c,A}}{1 - c_{sat}/(100 n_w M_w/M_{anh})}. \tag{22}$$

The rest of the salt (m_{diss}) is dissolved in the saturated solution. The average volume fraction occupied by the salt crystals is

$$\phi_c = \frac{m_c}{\rho_c V}, \tag{23}$$

where V is the total volume of the sample and ρ_c is the density of the salt crystal.

Experimental results

Material characterization

Figure 2 shows that the pores in HL are smaller than in IL, while 35 % of the porosity of IL consists of pores larger than 10 μm, 86 % of the porosity of HL lies in the range from 0.1 to 10 μm. HL has a significant amount of large macropores (in the mm range) that are not measured by mercury porosimetry.

The porosities determined after vacuum impregnation are larger than those obtained by saturation under atmospheric pressure (called capillary porosity P) (Table 2). This is caused by trapped air, which might result from large pores (where the air remains trapped) being connected through a network of smaller pores. This difference is more pronounced in HL (~ 13 vol%) than in IL (~ 3 vol%). The measured water sorptivity of HL [0.029 ± 0.004 cm^3/(cm^2 min$^{1/2}$)] is smaller than that of IL [0.047 ± 0.005 cm^3/(cm^2 min$^{1/2}$)], which is in agreement with the smaller size of the pores in HL and the expected higher resistance to capillary uptake. Thus, although the capillary rise height is larger in materials with small pores than with large pores (for the same porosity), the flow rate decreases with the pore size as expected from Poseuille's law or Eq. (8) (i.e., the uptake proceeds more slowly in a stone with smaller pores).
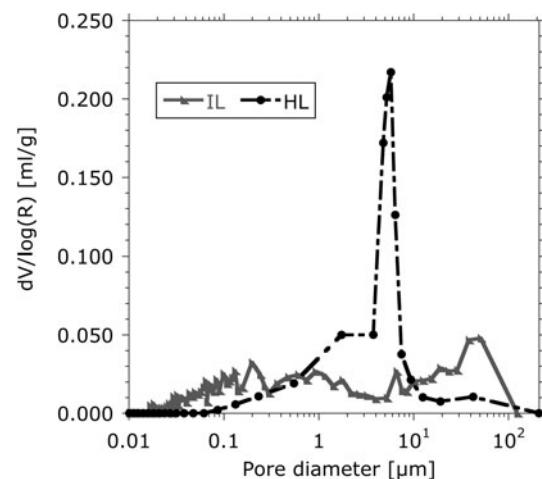
Fig. 2 Pore size distribution of Highmoor magnesian limestone (HL) and Indiana limestone (IL)

Table 2 Water saturation data of IL and HL

	IL	HL
Water saturation under atmospheric pressure (vol%)	11.7 ± 0.8	11.8 ± 0.4
Water saturation after vacuum (vol%)	14.5 ± 0.5	24.3 ± 1.5

Drying of capillary-saturated stone with salt solution

The experimental results of the drying experiments for IL were discussed by Espinosa-Marzal and Scherer (2008b); Fig. 3 shows the corresponding decrease of the water content with time. The water-saturated samples were completely dried after ∼14 days, and the samples impregnated with the SS solution achieved a constant weight after 28 days; however, a considerable amount of water remained in the samples. In contrast, the samples impregnated with SC and with MS solutions continued drying slowly after 80 days. The expected final mass of water after complete drying of the samples impregnated with MS is 0.14 wt%, corresponding to the water bound in kieserite ($MgSO_4 \cdot 1H_2O$), which is the stable phase at 21 °C and 31 % RH (Steiger et al. 2007). In the SC-contaminated samples, the expected amount of water in equilibrium is zero. Thus, a non-negligible amount of water remained in the pores of all samples, the highest amount being retained in the samples impregnated with MS. Efflorescences of SS (thenardite) were removed at the end of the drying experiment and the weight was determined, while no efflorescences were observed for either SC or MS.

Figure 4 shows the decreasing amount of water in the HL samples impregnated with water and with the salt solutions. The water-saturated HL samples were completely dry after 10 days, faster than IL. The HL samples
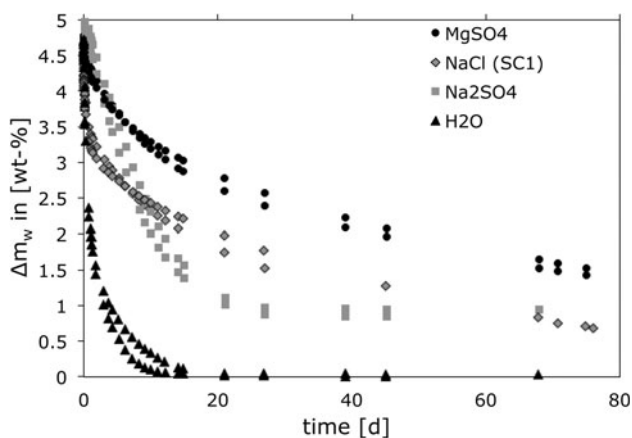

Fig. 3 Water content in IL during the drying at 31 % RH and 21 °C. The stone samples were initially impregnated with water, magnesium sulfate, sodium chloride (SC1) and sodium sulfate. The initial weight gives the mass of the adsorbed water
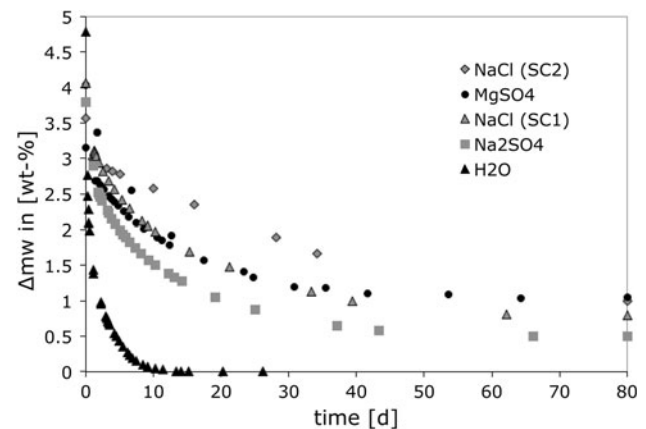

Fig. 4 Water content in HL during the drying at 31 % RH and 21 °C. The stone was initially impregnated with water, magnesium sulfate, sodium chloride (SC1 and SC2) and sodium sulfate. The water content remains constant in all samples after 8 months continuous drying under the same conditions

impregnated with salt solution achieved a constant weight within ∼65 days; the water content in HL was still constant after 8 months of drying under the same conditions. In contrast, the drying of IL with MS and SC continued after 80 days, as indicated by the still decreasing water content; a plateau has been achieved for the water content only in IL with SS. The most significant decrease of the drying rate of HL samples is caused by salt solution SC2. The drying of HL is more strongly hindered by the presence of MS and SC than that of IL, while the opposite trend is obtained for SS.

Drying of bulk solution

To determine the phase precipitated, droplets of the solutions were dried in a cooling stage on an optical microscope. Representative results are depicted in Fig. 5b, c. The concentration of MS decreased extremely slowly after reaching 3.8 m in the accompanying gravimetric experiments. The evaporation rate is determined by the gradient of vapor pressure, which is affected by the concentration-dependent water activity of the solution. At 21 °C the water activity for mirabilite is ≥94 %, for epsomite ≥91 % and for hexahydrite ≥85 % and therefore a smaller evaporation rate can be expected for highly concentrated MS solutions than for high-concentrated SS solutions. However, this cannot explain the negligible drying rate of MS. Indeed, the recorded images show that a thin layer of crystals formed at the liquid–air interface within 5–8 min (Fig. 5b), which hindered further drying, even after 27 days. At the achieved concentration, the crystallization of kieserite and starkeyite can be excluded, but both the epsomite and the metastable hexahydrite might have precipitated (Fig. 6).

Fig. 5 **a** Concentration and mass of water during the drying of droplets (∼25 μl) of magnesium sulfate (MS20) and sodium sulfate (SS12) at 31 % RH and 21 °C. The solubilities of epsomite, hexahydrite and starkeyite in mol/kg are indicated in the diagram by *lines*. **b** Dense surface layer of epsomite crystals formed at the liquid–gas interface. **c** Thenardite crystals precipitate directly from the supersaturated solution
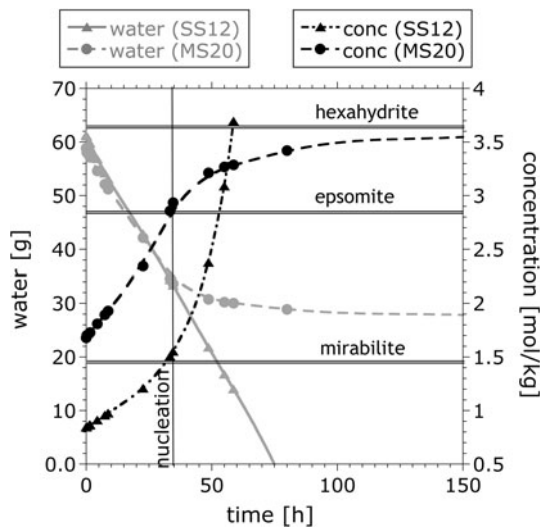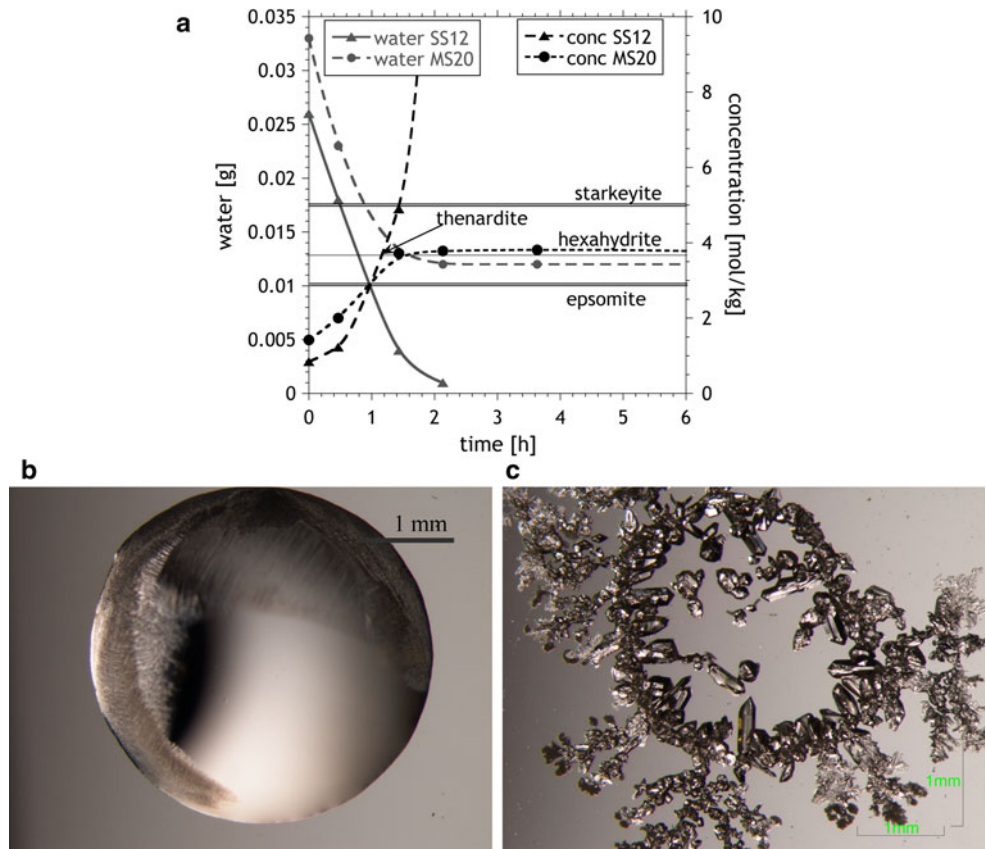

Fig. 6 Concentration and mass of water during the drying of bulk solutions of magnesium sulfate (MS20) and sodium sulfate (SS12) at 31 % RH and 21 °C contained in Petri dishes (diameter = 10 cm, solution volume = 90 ml). The solubilities of epsomite, hexahydrite and starkeyite in mol/kg are indicated in the diagram by *lines*. Epsomite and mirabilite nucleate at their respective saturation concentrations

The concentration of SS reached the solubility limit of thenardite after 1.25 h (Fig. 5a), whereupon crystallization was observed. The first crystals formed close to the droplet boundary after 35 min, where the concentration was higher. Orthorhombic dipyramidal and elongated crystals were observed, corresponding to the equilibrium geometry of thenardite (Amirthalingam et al. 1977). These crystals grew in the solution, while efflorescence grew out of the solution (Fig. 5c, image after 5 h). The solution retreated from the center to the border of the drop due to evaporation. Considering the weight and concentration changes in Fig. 5a, it is concluded that thenardite precipitated in the droplet during drying at 31 % RH and 21 °C.

After ∼15 min of drying-induced crystallization of halite in a droplet (SC2), 1–3 cubic crystals formed in the droplet, starting on the droplet boundary; they continued growing as the water evaporated, until they occupied the original droplet volume. After 51 min, the remaining solution film evaporated and precipitation occurred over the limits of the original drop, in agreement with the results in Shahidzadeh-Bonn et al. (2008).

The drying rate of the stones is slowed by the transport through the pore network and by the gradual pore filling with crystals; consequently, the concentration of the pore solution increases more slowly than in the droplet experiments. To study the effect of a slower increase of the concentration, a second set of drying experiments of bulk solution contained in Petri dishes was performed at 31 % RH and 21 °C. Although the surface area was increased and with it the evaporation rate,

the area per unit volume of solution was smaller than in the droplets experiments and consequently the evaporated total mass of water per unit volume proceeded significantly more slowly. Figure 6 shows the increasing concentration and the decreasing amount of water in MS and SS solutions. During crystallization the solutions did not achieve supersaturation with respect to either hexahydrite or heptahydrate and thenardite, respectively. Large prismatic epsomite and mirabilite crystals formed overnight. Since the concentration increased slowly, the solution remained supersaturated with respect to mirabilite and epsomite so long that mirabilite and epsomite were able to precipitate. Mirabilite dehydrates slowly; after 70 h it had completely dehydrated to thenardite. Epsomite crystals formed mainly at the liquid–vapor interface, preventing complete drying of the solution and dehydration of the crystals during the 9-day duration of the experiment. These results show that crystallization is influenced not only by the evaporation rate (Rodriguez-Navarro and Doehne 1999) as determined by the relative humidity and temperature of the surrounding air but also by the time-dependent evolution of the solution concentration (which depends on the relative rates of advection and diffusion of salt, and the geometry of the system) and the kinetics of nucleation.

The drying rate of the stones is reduced by the presence of crystals in the pores, which reduce the porosity and raise the tortuosity of the pore network. Whereas thenardite precipitates initially close to the drying surface of the stones, the droplet experiments indicate that mirabilite is more prone to precipitate within the stone as drying progresses and the evaporation rate diminishes and to slowly dehydrate to thenardite. Similarly, epsomite can be expected to precipitate within the stone, but its dehydration is strongly hindered (Balboni et al. 2011).

Estimation of the average precipitated salt content in the stones during drying

Table 3 shows the volume fraction of salt (ϕ_c) that precipitated in HL and IL calculated with the measured mass

of residual water m_w^{exp} and with Eq. (23), assuming that the salt is distributed uniformly in the specimen. Tables 3 and 4 also give the fraction of the pore volume occupied by the crystals (denoted "pore filling") $s_c = \phi_c/f_B$, where f_B is the capillary porosity of the salt-free material (11.7 % for IL and 11.8 % for HL) and s_{tot} the total pore fraction occupied by the crystals and the solution, assuming that the remaining solution at the end of the drying experiment is saturated at 21 °C.

There is an uncertainty about the content of mirabilite and thenardite in the stones, due to the ease with which mirabilite can dehydrate in the bulk experiments. Within the stone, the dehydration will be slowed due to the hindered vapor transport through the pores that gradually fill with crystals. Therefore, two extreme cases were calculated. It was first assumed that mirabilite alone was present in the pores of the stone to determine the maximal volume fractions occupied by the salt (viz., 2.33 vol% of mirabilite precipitated in IL). The measured amount of retained water is 0.90 wt%, of which 0.83 wt% is bound in mirabilite. The difference (0.07 wt%) gives the liquid water that remains in the specimen. The smallest volume fraction (0.76 vol%) is achieved by assuming that mirabilite completely dehydrates to thenardite. The real pore filling must lie between these limits. The formation of heavy thenardite efflorescence in IL indicates dehydration of mirabilite. The same estimation was performed for SS in HL. Mixtures of mirabilite and thenardite (40 and 30 % of thenardite in IL and HL, respectively) were assumed for the estimation, based on the results of "Sorptivity test with decane", as explained in "Discussion".

The maximal amount of precipitated epsomite in HL and IL is determined by neglecting dehydration, on the basis of the bulk experiments and the absence of efflorescence, and assuming that the solution is saturated with respect to epsomite at the end of the experiment. The corresponding values for SC1 and SC2 were calculated assuming that the residual solution in the stone is saturated with respect to halite.

Table 3 Volume fraction occupied by the precipitated salt in IL (ϕ_c), pore filling with salt crystals s_c, total pore filling including the volume occupied by the solution s_{tot}, gravimetrically measured remaining mass of water (m_w^{exp}) and maximal mass of crystal water ($m_{w,c}^{max}$)

2IL	ϕ_c (vol%)	s_c (%)	s_{tot} (%)	m_w^{exp} (wt%)	$m_{w,c}^{max}$ (wt%)
2IL-MS20					
Epsomite	1.90	16.24	29.9	1.48	0.71
2IL-SS12					
Mirabilite	2.33	19.8	20.9	0.90	0.83
Thenardite	0.76	6.42	19.4	0.90	0
Mirabilite (60 %)/thenardite (40 %)	1.27	10.7	19.6	0.90	0.37
2IL-SC1					
Halite	0.69	5.90	17.4	0.57	0

Table 4 Volume fraction occupied by the precipitated salts in HL (ϕ_c), pore filling with salt crystals (s_c), total pore filling including the volume occupied by the solution (s_{tot}), gravimetrically measured residual mass of water (m_w^{exp}) and maximal mass of hydration water ($m_{w,c}^{max}$)

	ϕ_c (Vol%)	s_c (%)	s_{tot} (%)	m_w^{exp} (wt%)	$m_{w,c}^{max}$ (wt%)
MS20					
Epsomite	1.82	15.4	22.3	1.09	0.73
SS12					
Mirabilite	1.33	11.8	11.8	0.51	0.51
Thenardite	0.30	2.33	11.3	0.51	0
Mirabilite (70 %)/ thenardite (30 %)	1.21	10.3	12.3	0.51	0.39
SC2					
Halite	0.84	7.1	27.8	1.00	0
SC1					
Halite	0.47	4.0	20.4	0.79	0

In all experiments, a small volume fraction of precipitated salt ($\phi_c < 2$ vol%) is observed, which means that the pore filling $s_c < 17$ %. The highest volume fraction of precipitated salt is reached in IL with epsomite, followed by the mixture of mirabilite and thenardite and by halite (SC1). The amount of residual water indicates that the drying is most significantly retarded by MS salts and least by halite (SC1). The IL samples impregnated with SC2 could not be evaluated, since the growing halite crystals perforated the coating, which accelerated the drying.

In HL, the highest volume fraction of precipitated salt is reached by epsomite, followed by the mixture of mirabilite and thenardite, and by halite (SC2 and SC1). The amount of remaining water indicates that the hindered drying induced by halite (SC2) and by epsomite is very similar (1.09 vs 1.00 vol%), but the pore volume occupied by the halite crystals is much smaller and consequently the pore clogging is comparatively more efficient. Therefore, there is no direct correlation between volume fraction of precipitated salt and decrease in drying rate in HL.

Sorptivity test with decane

The results of the sorptivity test with decane for IL and HL are depicted in Figs. 7 and 8, respectively (data points). The imbibition i is defined as the cumulative volume of the adsorbed liquid per unit area of inflow surface. Both figures show that the capillary uptake of decane does not follow the $\sqrt{t}$ course strictly, if salt has precipitated within the pores. The slope of the imbibition curves increases progressively, indicating a decrease in the resistance to flow with increasing uptake. According to the model of a bilayer composite (Hall and Hoff 2002), this means that the
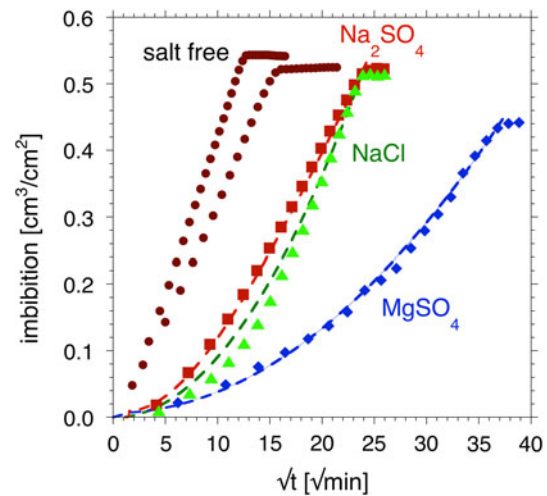

Fig. 7 Measured imbibition i of decane in the salt-free samples of IL and in the samples with halite (0.69 vol%, SC1), mirabilite/thenardite (1.27 vol%) and epsomite (1.90 vol%), respectively, after the drying experiment (data points). The *lines* give the calculated imbibition for the best fit between Eq. (14) and experimental results. The results were obtained in different samples of IL from the same block
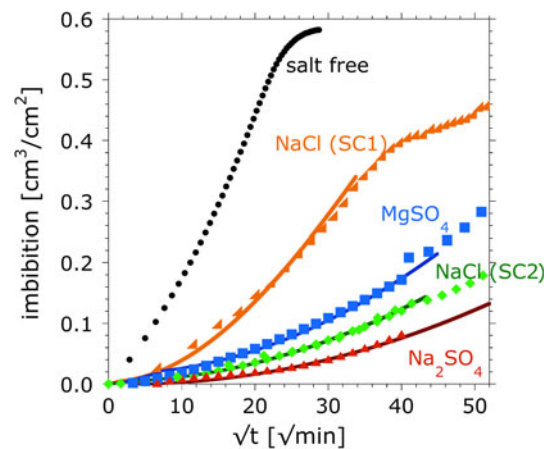

Fig. 8 Computed and measured imbibition of decane in HL salt-free samples and with 0.47 vol% halite (SC1), 0.84 vol% halite (SC2), 1.21 vol% mirabilite/thenardite and 1.82 vol% epsomite. The experimental results were obtained in different samples of HL from the same block

resistance to the capillary uptake close to the wet surface is more significant than that of the bare stone, due to the precipitated salts.

In the case of SS in IL (Fig. 7), there is an initial delay in the uptake of decane, but after 2 h the difference of the slope with respect to the bare stone becomes lower. Similar results are obtained for halite. The uptake in the salt-contaminated samples is more strongly reduced in HL than in IL, compared to the salt-free stone, which demonstrates the more intensive pore clogging by the precipitated salts in HL, which is the stone with the smaller pores and lower

sorptivity. The measurements were interrupted after 48 h, before saturation was achieved. The uptake in the presence of MS salts proceeds very slow in both stones despite their different pore structure.

Discussion

The low volume fraction of salt shown in Tables 3 and 4 can hardly explain the strongly retarded decane uptake. The amount of residual water during drying cannot be correlated with the slowdown of the capillary uptake; for example, the mixture of mirabilite and thenardite in HL leads to a small residual water content, but the pore clogging during decane uptake is very significant (see data points in Fig. 8). Moreover, very effective resistance to decane uptake is induced by SS salts, epsomite, and halite (SC2) in HL (Fig. 8), and the resistance induced by the different salts is of the same order despite the different pore filling of these salts in HL (from 4 to 15.4 vol%; Table 4).

In fact, the average pore filling does not account for the pore clogging induced by the precipitated salts, since salt does not precipitate uniformly within the sample, but is concentrated close to the drying surface (Huinink et al. 2002; Pel et al. 2002; Sghaier et al. 2007), as also indicated by the anomalous decane imbibition. By fitting Eq. (14) to the experimental results, it is possible to determine the width of the crystallization front (L_A) and the pore filling within the crystallization front S_c^A; the only fitting parameter is L_A. Figure 9 shows the results for both stones. The pore filling within the crystallization front is very high and similar (~ 98 %) for all three salts in IL. The point of inflection in Fig. 7 is at about 0.06–0.07 cm ($\sim i_A$), which is obtained with Eq. (14) if 30–40 % of mirabilite has dehydrated to thenardite. This thenardite content was assumed for the calculations in Table 3. Similarly, during the decane uptake in HL the inflection point is at ~ 0.06 cm ($\sim i_A$) (Fig. 8). This is obtained by assuming that ~ 30 % of the mirabilite dehydrates to thenardite, which was assumed for the calculations in Table 4 and in Fig. 8. In this stone, the highest pore filling is achieved by mirabilite (~ 96 %), consistent with the slowest decane imbibition.

The calculated pore filling in HL is smaller than that obtained for IL, although the pore clogging is more intense in HL during decane imbibition. This can be explained by the influence of the pore size distribution: crystallization in small pores that serve as entries to large pores leads to an intense pore clogging (for the transport) at a lower pore filling. Since HL is the stone with more small pores, this situation is more likely in HL than in IL.

Figure 7 compares the computed imbibition of the salt-contaminated IL samples (dotted lines) with the experimental results. Representative results for each salt have
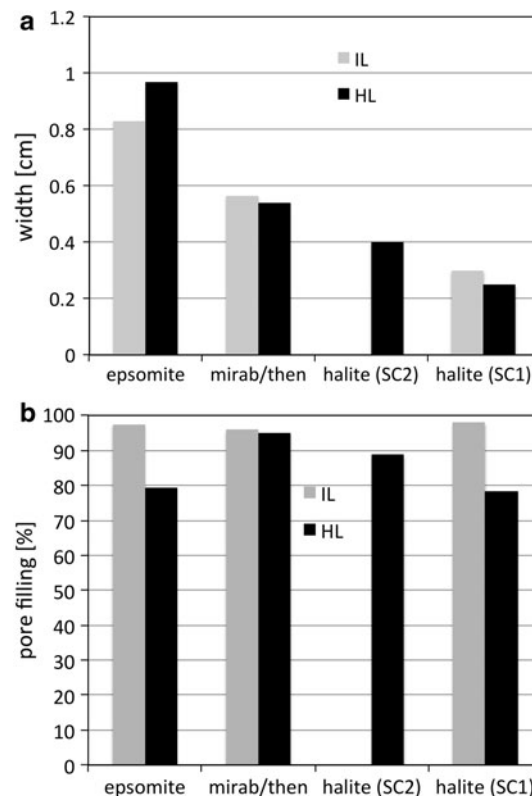

Fig. 9 **a** Width of the crystallization front and **b** pore filling within the crystallization front obtained from the best fit between measured imbibition and Eq. (14) assuming cylindrical pores

been selected. Very good agreement between measured and computed decane imbibition is obtained for SS and MS salts. The calculated sorptivity converges with progressing imbibition to that of the salt-free material, which must be higher than that of the salt-contaminated material. Figure 8 shows very good agreement between experimental and computed imbibition for HL. The uptake is slow and the transition into the imbibition through the salt-free material is not achieved within the duration of the experiment (48 h). For decane uptake in HL with SS only one measurement was performed, which was interrupted due to a power failure.

Strong differences in the crystallization behavior of the three selected salts were observed in bulk solution that aid in understanding the salt-dependent discrepancies observed in the two limestones. The smallest crystallization front width is achieved by halite, but Fig. 8 demonstrates that the pore clogging is not directly correlated to it (e.g., compare results for SC2 and MS in HL). SEM images of the drying-induced crystallization of halite (Benavente et al. 2004) indicate that halite crystals grow within the pores until virtually filling them, causing a significant pore clogging that blocks further transport of solution. The pore clogging induced by MS is very likely related to the formation of a dense layer of epsomite crystals at the liquid–vapor

interface, which was observed in the bulk experiments, and has not been previously reported. This layer would impede further drying, and therefore explain why the pore clogging is very effective in both stones, despite their different pore structures. The width of the crystallization front of epsomite in both stones is the highest ($\sim$0.83–0.97 cm), which is also consistent with the high viscosity of the solution; the slower capillary transport of the highly viscous solution moves the drying front further into the interior of the specimen (Scherer 2004).

The large amount of bound water in mirabilite, together with its high molar volume, accounts for the pore clogging induced by SS salts. The strong difference in pore clogging induced by mirabilite/thenardite in IL and HL indicates the influence of the pore size distribution, i.e., that the presence of smaller pores promotes pore clogging. In the field it is to be expected that the ease of the dehydration of mirabilite to thenardite gradually re-opens the pore system.

The imbibition analysis was performed by assuming the existence of a sharp interface between the salt-free material and the crystallization front, and a uniform salt distribution within the crystallization front. Moreover, the reduction of the porosity was modeled by considering the decrease of the average pore radius, assuming cylindrical pores. Indeed, it is more realistic to expect a gradient of the precipitated salt within the crystallization front and a pore-size-dependent salt distribution. It can be expected that large pores can be blocked against decane transport if salt precipitates in the small entries, causing intensive pore clogging at a low degree of pore filling. This is likely the reason for the significant pore clogging during decane imbibition, in spite of low pore filling in HL compared to IL, since HL has a larger amount of smaller pores. However, to prove the influence of the pore size distribution on pore clogging, direct visualization of crystals in the pore network is necessary. Unfortunately, optical microscopy or ESEM only show crystals forming on the surface, and not in the pores within the material, which is of ultimate interest. Material fracture for imaging of crystals in pores or MIP would expose salt to a different environment (air) and induce phase changes by dehydration of existing phases and precipitation from residual liquid. A direct assessment of crystallization in the pore network might soon be possible by X-ray tomography due to the steadily increasing resolution (Derluyn et al. 2012).

It is not known yet whether pore clogging will enhance or reduce damage to stone from salt crystallization. Different scenarios suggest the influence of pore clogging on damage, though. If pore clogging exists within the drying front, a decrease of temperature can lead to supersaturation of the residual solution, which is present as a thin film between the crystals, and between the salt and the pore walls. Since crystal growth cannot continue, due to spatial confinement,

an increase of the crystallization pressure might be induced. Moreover, the pressure caused by freezing of water in pores whose entrances are clogged with salt crystals might cause significant damage. Finally, the high thermal expansion of salt can create destructive stresses during heating of stone with salt-filled pores (Larsen and Nielsen 1990). On the other hand, less pore clogging maintains the drying rate higher and consequently it is more likely to displace the crystallization front deeper into the material (Scherer 2004), raising the supersaturation and causing the formation of subflorescence. Prediction and prevention of salt damage is possible only if the interaction between material properties, environmental conditions, and composition of the solid (minerals) and fluid phases are considered. Thus, to describe the complexity of salt weathering, a computational tool that includes these interacting phenomena is required. We are currently developing such a numerical model, called ASTRA (Franke et al. 2007), which has already been successfully applied to understand factors influencing salt damage in simple laboratory experiments (see, e.g., (Espinosa-Marzal and Scherer 2009; Espinosa-Marzal et al. 2011).

Conclusions

The influence of three different salts (NaCl, MgSO$_4$ and Na$_2$SO$_4$) on the drying rate at constant temperature and relative humidity was studied in two materials with different pore structures. The results show a very intensive slowing down of the drying rate, compared to that of water-saturated stone and a high amount of residual water.

Evidence for pore clogging induced by the precipitated salts is obtained by measuring the capillary uptake of decane through the crystallization front. This experiment shows that pore clogging is induced by the crystallization of halite, thenardite/mirabilite, and epsomite in both stones, despite the small total salt content (<2 vol%). A sharp-front analysis of the uptake rate of decane indicates that the precipitated salts induce a very high pore filling in both stones within a narrow crystallization front of less than 1 cm, which accounts the strong retardation of the drying rate.

Pore clogging is strongly dependent on the type of salt and the pore structure of the host. Our results indicate that materials with small pores are more prone to pore clogging. However, the particular salt behavior can dominate over the pore structure. In case of MS, the resistance to flow is related to the formation of a dense layer of epsomite crystals at the liquid–vapor interface that impedes further drying (as well as subsequent capillary uptake) in materials with different pore size distribution. Mirabilite dehydrates more readily than magnesium salts, which allows partially reopening of blocked pores.

To predict damage from salt crystallization, it will be necessary to obtain more precise information about the location of the salt within the pore network. Unfortunately, the current spatial resolution of tomographic techniques is not yet sufficient for this purpose.

References

Amirthalingam V, Karkhanavala MD, Rao URK (1977) Topotaxic phase-change in Na_2SO_4. Acta Crystallogr A 33:522

Balboni E, Espinosa-Marzal RM, Doehne E, Scherer GW (2011) Can drying and re-wetting of magnesium sulfate salts lead to damage of stone? Environ Earth Sci 63(7–8):1463–1473. doi:10.1007/S12665-010-0774-1

Benavente D, Garcia del Cura MA, Garcia-Guinea J, Sanchez-Moral S, Ordoñez S (2004) Role of pore structure in salt crystallisation in unsaturated porous stone. J Cryst Growth 260:532–544. doi:10.1016/j.jcrysgro.2003.09.004

Correns CW (1949) Growth and dissolution of crystals under linear pressure. Discuss Faraday Soc 5:267–271

Derluyn H, Griffa M, Mannes D, Jerjen I, Dewanckele J, Vontobel P, Sheppard A, Boone M, Derome D, Cnudde V, Lehmann E, Carmeliet J (2012) Probing salt crystallization damage mechanisms in porous limestone with neutron radiography and X-ray tomography. Proceedings of the 5th International Building Physics Conference, 5th IBPC Organizing Committee, pp 95–102

Doehne E, Pinchin S (2008) Time-lapse macro-imaging in the field: monitoring rapid flaking of magnesian limestone. In: Lukaszewicz J, Niemcewicz P (eds) Proceedings of the 11th international congress on deterioration and conservation of stone, Torun Nicolaus Copernicus University Press, Torun, pp 365–372

Espinosa-Marzal RM, Scherer GW (2008a) Crystallization of sodium sulfate salts in limestone. Environ Geol 56(3–4):605–621. doi:10.1007/S00254-008-1441-7

Espinosa-Marzal RM, Scherer GW (2008b) Study of the pore clogging induced by salt crystallization in Indiana limestone. Proceedings of the 11th International Congress on Deterioration and Conservation of Stone, Nicolaus Copernicus University Press, Torun, pp 81–88

Espinosa-Marzal RM, Scherer GW (2009) Crystallization pressure exerted by in-pore confined crystals. Poromechanics 4:1013–1018

Espinosa-Marzal RM, Hamilton A, McNall M, Whitaker K, Scherer GW (2011) The chemomechanics of crystallization during rewetting of limestone impregnated with sodium sulfate. J Mater Res 26(12):1472–1481. doi:10.1557/Jmr.2011.137

Evans IS (1969) Salt crystallization and rock weathering. Rev Géomorphologie dynamique XIX 4:153–177

Flatt RJ (2002) Salt damage in porous materials: how high supersaturations are generated. J Cryst Growth 242(3–4):435–454. doi:10.1016/s0022-0248(02)01429-x

Flatt R, Steiger M, Scherer G (2007) A commented translation of the paper by C.W. Correns and W. Steinborn on crystallization pressure. Environ Geol 52(2):187–203. doi:10.1007/s00254-006-0509-5

Foster W, Hoover KW (1963) Hexahydrite ($MgSO4\cdot6H2O$) as an efflorescence of some Ohio dolomites. Ohio J Sci 63:152–158

Franke L, Kiekbusch J, Espinosa R, Gunstmann C (2007) CESA and ASTRA—two program systems for cement and salt chemistry and the prediction of corrosion processes in concrete. Proceedings of International Conference on Durability of HPC and Final Workshop of CONLIFE, Aedificatio Publishers, Essen, p 501

Goudie A, Viles H (1997) Salt weathering hazards. Wiley, Chichester

Guglielmini L, Gontcharov A, Aldykiewicz AJ, Stone HA (2008) Drying of salt solutions in porous materials: intermediate-time dynamics and efflorescence. Phys Fluids 20(7):077101. doi:10.1063/1.2954037

Hall C, Hoff W (2002) Water transport in brick, stone and concrete. Spon Press, London

Happel J, Brenner H (1983) Low Reynolds number hydrodynamics. Springer, Netherlands

Huinink HP, Pel L, Michels MAJ (2002) How ions distribute in a drying porous medium: a simple model. Phys Fluids 14(4):1389–1395

Janssen H, Derluyn H, Carmeliet J (2012) Moisture transfer through mortar joints: a sharp-front analysis. Cement Concrete Res 42(8):1105–1112. doi:10.1016/j.cemconres.2012.05.004

Kirk JW, Dobbs JB (2002) A Protocol to inhibit the formation of natrium chloride salt blocks. Proceedings of the International Symposium on Oilfield Scale, Aberdeen, pp 1–5 doi:10.2118/74662-MS

Larsen E, Nielsen C (1990) Decay of bricks due to salt. Mater Struct 23(1):16–25. doi:10.1007/bf02472994

Lide DR (2006–2007) CRC handbook of chemistry and physics. 87th edn. CRC Press, Boca Raton. http://www.hbcpnetbase.com

Lopez-Arce P, Garcia-Guinea J, Benavente D, Tormo L, Doehne E (2009) Deterioration of dolostone by magnesium sulphate salt: an example of incompatible building materials at Bonaval Monastery. Spain Constr Build Mater 23(2):846–855. doi:10.1016/j.conbuildmat.2008.04.001

Pel L, Huinink H, Kopinga K (2002) Ion transport and crystallization in inorganic building materials as studied by nuclear magnetic resonance. Appl Phys Lett 81(15):2893–2895. doi:10.1063/1.1512329

Prat M (2007) On the influence of pore shape, contact angle and film flows on drying of capillary porous media. Int J Heat Mass Transf 50(7–8):1455–1468. doi:10.1016/j.ijheatmasstransfer.2006.09.001

Rodriguez-Navarro C, Doehne E (1999) Salt weathering: influence of evaporation rate, supersaturation and crystallization pattern. Earth Surf Proc Land 24(3):191–209

Ruiz-Agudo E, Mees F, Jacobs P, Rodriguez-Navarro C (2007) The role of saline solution properties on porous limestone salt weathering by magnesium and sodium sulfates. Environ Geol 52(2):305–317. doi:10.1007/S00254-006-0476-X

Samson E, Marchand J (2007) Modeling the transport of ions in unsaturated cement-based materials. Comput Struct 85(23–24):1740–1756. doi:10.1016/j.compstruc.2007.04.008

Scherer GW (2004) Stress from crystallization of salt. Cem Concr Res 34(9):1613–1624. doi:10.1016/j.cemconres.2003.12.034

Sghaier N, Prat M (2009) Effect of efflorescence formation on drying kinetics of porous media. Transp Porous Media 80(3):441–454. doi:10.1007/s11242-009-9373-6

Sghaier N, Prat M, Nasrallah S (2007) On ions transport during drying in a porous medium. Transp Porous Media 67(2):243–274. doi:10.1007/s11242-006-9007-1

Shahidzadeh-Bonn N, Rafai S, Bonn D, Wegdam G (2008) Salt crystallization during evaporation: impact of interfacial properties. Langmuir 24(16):8599–8605. doi:10.1021/La8005629

Shahidzadeh-Bonn N, Desarnaud J, Bertrand Fo, Chateau X, Bonn D (2010) Damage in porous media due to salt crystallization. Phys Rev E 81(6):066110

Shokri N, Lehmann P, Or D (2010) Liquid-phase continuity and solute concentration dynamics during evaporation from porous media: pore-scale processes near vaporization surface. Phys Rev E 81(4):046308. doi:10.1103/Physreve.81.046308

Steiger M (2005a) Crystal growth in porous materials I: the crystallization pressure of large crystals. J Cryst Growth 282(3–4):455–469. doi:10.1016/J.Jcrysgro.2005.05.007

Steiger M (2005b) Crystal growth in porous materials II: influence of crystal size on the crystallization pressure. J Cryst Growth 282(3–4):470–481. doi:10.1016/J.Jcrysgro.2005.05.008

Steiger M, Siegesmund S (2007) Special issue on salt decay. Environ Geol 52(2):185–186. doi:10.1007/s00254-006-0591-8

Steiger M, Linnow K, Juling H, Gülker G, Jarad AE, Brüggerhoff S, Kirchner D (2007) Hydration of $MgSO_4 \cdot H_2O$ and generation of stress in porous materials. Cryst Growth Des 8(1):336–343. doi:10.1021/cg060688c

Steiger M, Kiekbusch J, Nicolai A (2008) An improved model incorporating Pitzer equations for calculation of thermodynamic properties of pore solutions implemented into an efficient program code. Constr Build Mater 22(8):1841–1850. doi:10.1016/j.conbuildmat.2007.04.020

Wang A, Freeman JJ, Jolliff BL (2009) Phase transition pathways of the hydrates of magnesium sulfate in the temperature range 50 °C to 5 °C: implication for sulfates on Mars. J Geophys Res 114(E04010):1–28. doi:10.1029/2008je003266

Wesson JA, Worcester EM, Wiessner JH, Mandel NS, Kleinman JG (1998) Control of calcium oxalate crystal structure and cell adherence by urinary macromolecules. Kidney Int 53(4):952–957